

Article

Activation of Peracetic Acid by CoFe_2O_4 for Efficient Degradation of Ofloxacin: Reactive Species and Mechanism

Rong Li, Xing Lu, Jinxiang Gao, Yifan Chen and Shunlong Pan * 

School of Environmental Science and Engineering, Nanjing Tech University, Nanjing 211816, China; 202161202058@njtech.edu.cn (R.L.); 202161102009@njtech.edu.cn (X.L.); 202261202027@njtech.edu.cn (J.G.); 202261202055@njtech.edu.cn (Y.C.)

* Correspondence: shunlongpan@njtech.edu.cn

Abstract: Peroxyacetic acid (PAA)-based advanced oxidation processes (AOPs) have attracted much attention in wastewater treatment by reason of high selectivity, long half-life reactive oxygen species (ROS), and wider applicability. In this study, cobalt ferrite (CoFe_2O_4) was applied to activate PAA for the removal of ofloxacin (OFX). The degradation of OFX could reach 83.0% via the CoFe_2O_4 /PAA system under neutral conditions. The low concentration of co-existing anions and organic matter displayed negligible influence on OFX removal. The contributions of hydroxyl radicals ($\cdot\text{OH}$), organic radicals ($\text{R}\cdot$), and other reactive species to OFX degradation in CoFe_2O_4 /PAA were systematically evaluated. Organic radicals (especially $\text{CH}_3\text{C}(\text{O})\text{OO}\cdot$) and singlet oxygen ($^1\text{O}_2$) were verified to be the main reactive species leading to OFX destruction. The $\text{Co}(\text{II})/\text{Co}(\text{III})$ redox cycle occurring on the surface of CoFe_2O_4 played a significant role in PAA activation. The catalytic performance of CoFe_2O_4 remained above 80% after five cycles. Furthermore, the ecotoxicity of OFX was reduced after treatment with the CoFe_2O_4 /PAA system. This study will facilitate further research and development of the CoFe_2O_4 /PAA system as a new strategy for wastewater treatment.

Keywords: peroxyacetic acid; cobalt ferrite; organic radicals; singlet oxygen; fluoroquinolone antibiotics



Citation: Li, R.; Lu, X.; Gao, J.; Chen, Y.; Pan, S. Activation of Peracetic Acid by CoFe_2O_4 for Efficient Degradation of Ofloxacin: Reactive Species and Mechanism. *Molecules* **2023**, *28*, 7906. <https://doi.org/10.3390/molecules28237906>

Academic Editor: Javier Llanos

Received: 3 November 2023

Revised: 26 November 2023

Accepted: 29 November 2023

Published: 2 December 2023



Copyright: © 2023 by the authors. Licensee MDPI, Basel, Switzerland. This article is an open access article distributed under the terms and conditions of the Creative Commons Attribution (CC BY) license (<https://creativecommons.org/licenses/by/4.0/>).

1. Introduction

Fluoroquinolones (FQs) are synthetic medicines with a broad antibacterial spectrum and potent antibacterial activity used in medicine and aquaculture. Only 30–70% of FQs are digested and absorbed by organisms and excreted directly into the ecosystem as natural or metabolites [1–3]. Currently, FQs have been widely detected in wastewater, surface water, groundwater, and even drinking water with trace concentrations ranging from ng/L to $\mu\text{g}/\text{L}$ [4]. FQs have attracted widespread public attention as a new environmental pollutant with the environmental risk of induced resistance genes [5]. Ofloxacin (OFX) is a typical representative of FQs and is hard to degrade in the natural environment [6]. Additionally, OFX could form chelates with some metal ions, resulting in more biotoxicity and resistance to degradation [7]. Therefore, it is essential to efficiently remove OFX from the aqueous environment. Advanced oxidation processes (AOPs) are promising methods for antibiotics in water due to the short reaction time and higher efficiency [8–11]. However, the availability of conventional AOPs is dependent on ideal pH and less interfering substance.

Peroxyacetic acid (PAA) has been widely utilized as a disinfectant, bleaching agent, sterilizer, oxidizing agent, and polymerization catalyst in the food processing, medical, chemical, and paper industries [12,13]. Compared with conventional disinfectants, PAA shows enhanced bactericidal ability, low pH dependence, flexible operation, and less toxicity via by-products [14]. Aside from its disinfectant properties, PAA possesses a high redox potential of 1.96 V, making it capable of degrading organic pollutants [13]. PAA can also be activated by UV irradiation, heat, and transition metal activation, producing reactive oxygen species (ROS) with high oxidation ability as a result, such as hydroxyl

radicals ($\cdot\text{OH}$) and organic radicals ($\text{CH}_3\text{C}(\text{O})\text{O}\cdot$, $\text{CH}_3\text{C}(\text{O})\text{OO}\cdot$), due to the fact that it has an easily activated O-O bond that is also contained in hydrogen peroxide (H_2O_2), peroxydisulfate (PDS), and peroxymonosulfate (PMS) [15,16]. The slight dependence on pH, anti-interference, and less disinfection byproducts are the more interesting features of PAA-based AOPs over conventional AOPs [17]. Moreover, transition metals are considered to be the optimal activation method due to their natural abundance, lack of external energy, and highly catalytic performance [18].

Co(II) is generally considered the most effective activator for PAA among the transition metals (e.g., Co(II), Fe(II), Mn(II), and Cu(II)) [16,19,20]. The mechanism of PAA activation by metal ions is shown in Equations (1) and (2) [21]. However, the poor reusability, secondary pollution, and toxicity of metal catalysts are the main hindrances to such homogeneous activation methods [20,22–24]. For this, developing heterogeneous cobalt catalysts for PAA activation is essential. Spinel ferrites are widely used as wave-absorbing materials and nanocomposite films due to their excellent stability and fascinating magnetic properties [25–27]. Additionally, they are also a good choice to serve as the catalytic material in AOPs. Recently, cobalt ferrite (CoFe_2O_4) has been demonstrated as an excellent PAA activator, owing to its strong structural stability, low metal ion leaching, bimetallic components, and magnetic properties [28–32]. As such, the application of CoFe_2O_4 in PAA activation might hold promise for the efficient degradation of FQs in wastewater. Even though the CoFe_2O_4 /PAA system has been studied for removing pollutants from water, there is limited information on what active species are present in the system and how CoFe_2O_4 activates PAA to specifically degrade contaminants.



This study aimed to assess the roles of reactive species of CoFe_2O_4 /PAA in degrading OFX and further elucidate its catalytic mechanism. Firstly, the degradation efficiency of OFX in the CoFe_2O_4 /PAA system was explored according to the effects of CoFe_2O_4 dosages, PAA concentration, initial pH, and water matrix (common anions and HA). Subsequently, the stability and reusability of CoFe_2O_4 on PAA activation were evaluated. Furthermore, the dominant reactive species in the CoFe_2O_4 /PAA system for OFX removal was identified. Finally, the degradation pathway of OFX and the toxicity of OFX before and after its treatment in the CoFe_2O_4 /PAA system were proposed.

2. Results and Discussion

2.1. Characterization of CoFe_2O_4

Figure 1a shows the XRD spectra of CoFe_2O_4 before and after the reaction. There are seven well-defined peaks in the XRD spectra, which confirm the crystal structure and excellent crystallinity of CoFe_2O_4 , and the diffraction peaks correspond to the characteristic peaks in the standard spectrum of CoFe_2O_4 . Moreover, the positions of the characteristic diffraction peaks of CoFe_2O_4 did not change before and after the reaction, indicating the great structural stability of CoFe_2O_4 . The FT-IR spectra of CoFe_2O_4 before and after the reaction are presented in Figure 1b. The absorption peaks nearing 3421 cm^{-1} and 1625 cm^{-1} correspond to the stretching and bending vibration of hydroxyl groups, respectively, which are mainly from surface-adsorbed water molecules [33]. Additionally, the peak nearing 580 cm^{-1} can be interpreted as a stretching vibration of metal–oxygen (M-O) and it could further verify the formation of Co/Fe-O [34]. Additionally, it is obvious that CoFe_2O_4 exhibits irregular particles with a size of about 100 nm (Figure 1c), and the elemental mapping image (Figure 1d) revealed that Co, Fe, and O were uniformly distributed on the surface of CoFe_2O_4 .

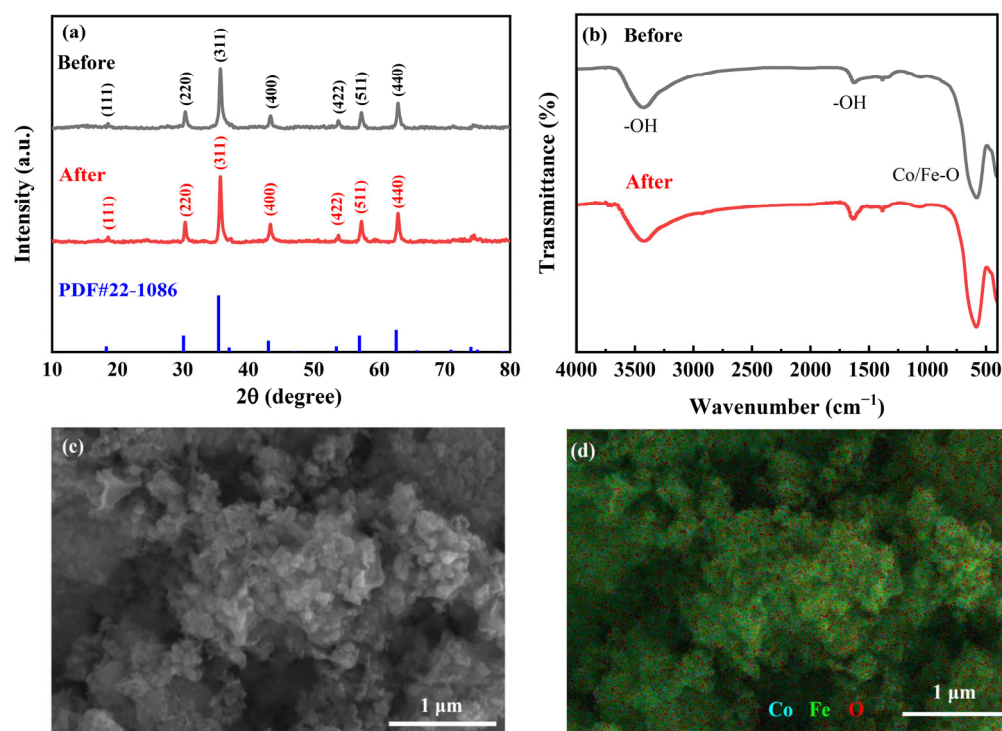


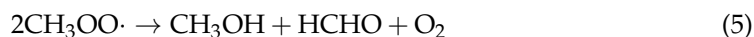
Figure 1. XRD spectra (a) and FT-IR spectra (b) of CoFe₂O₄ before and after the reaction. SEM image of CoFe₂O₄ (c) with the elemental mapping images of CoFe₂O₄ (d).

2.2. Performances of OFX Degradation by CoFe₂O₄-Activated PAA Oxidation

2.2.1. Degradation of OFX by the System of CoFe₂O₄/PAA

The degradation of OFX under different systems is shown in Figure 2a. OFX was almost not degraded in the system of H₂O₂ and PAA alone, indicating that it was negligible to oxidize OFX with H₂O₂ and PAA. Only 5.5% and 6.0% of OFX were removed by CoFe₂O₄ alone and the CoFe₂O₄/H₂O₂ system, respectively, suggesting that CoFe₂O₄ has weak physical adsorption capability to OFX and trouble activating H₂O₂. Compared with other systems, CoFe₂O₄ was able to degrade OFX effectively, and the removal rate reached 83.0% after 45 min, which implies that CoFe₂O₄ is an effective catalyst for PAA activation. This is due to the activation of PAA adsorption on the surface of CoFe₂O₄ and its decomposition to produce highly reactive radicals, which leads to the degradation of organic pollutants [17].

In addition, the decomposition of PAA during the reaction is displayed in Figure S1. Almost all of the PAA decomposed after 45 min. It is noteworthy that the catalytic decomposition of PAA can be accompanied by the production of a large number of fine carbon sources, including methanol (CH₃OH), acetic acid (CH₃COOH), and formaldehyde (HCHO) (Equations (3)–(6)) [16,17], and the PAA solution itself contains a certain amount of acetic acid, which can be used in the biological treatment process. Therefore, the CoFe₂O₄/PAA process in combination with biological treatment processes has great potential for application in the field of water treatment.



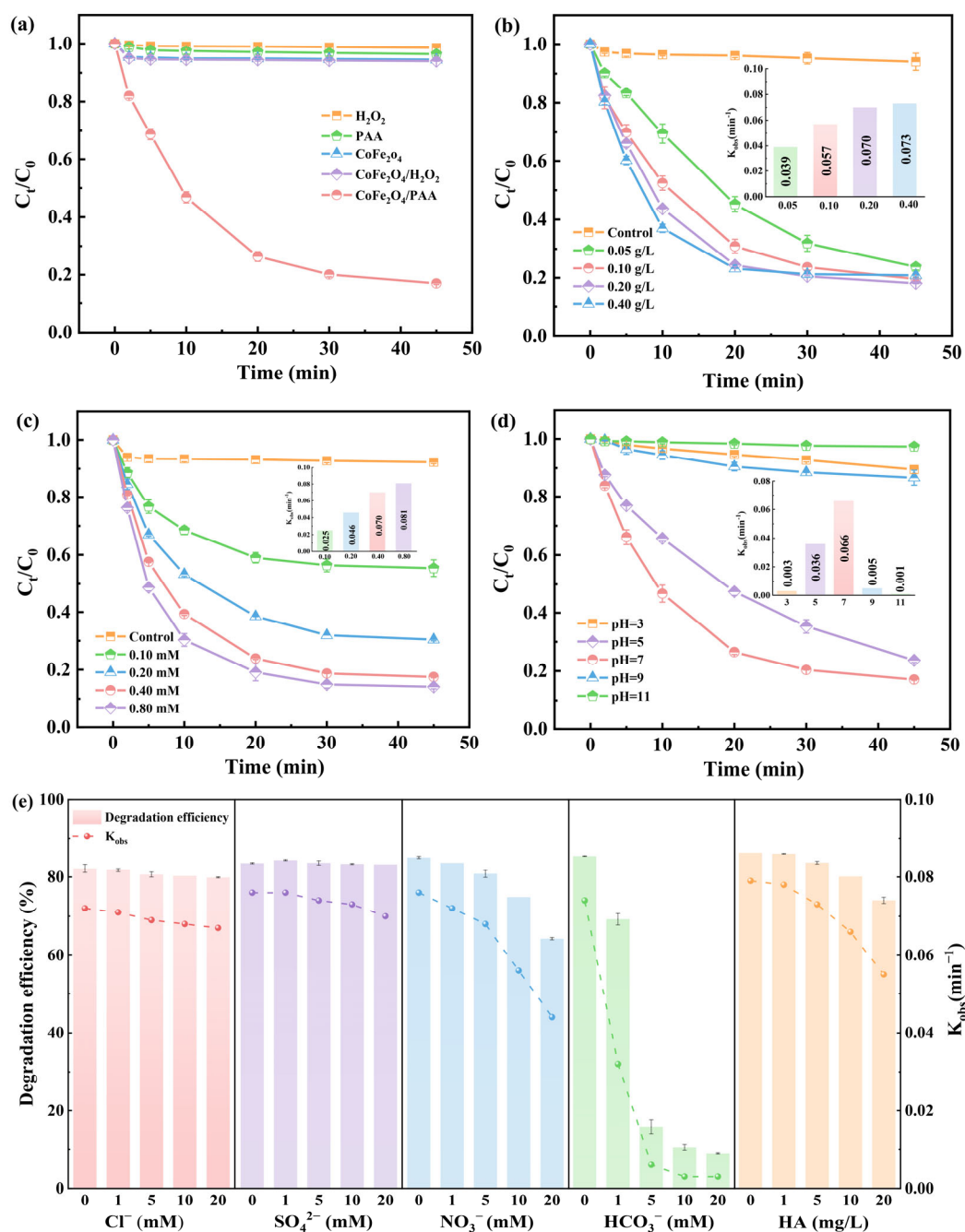


Figure 2. Degradation of OFX in different systems (a); the effect of reaction factors on the degradation of OFX in $CoFe_2O_4/PAA$ system, the inset figures show the corresponding kinetic constants: $CoFe_2O_4$ dosage (b), PAA concentration (c), initial pH (d), and the effect of water matrix on the degradation of OFX (Cl^- , SO_4^{2-} , NO_3^- , HCO_3^- , and HA) (e). Experimental conditions: $[OFX] = 20 \mu M$, $[PAA] = 0.4 \text{ mM}$, $[H_2O_2] = 0.6 \text{ mM}$, $CoFe_2O_4 = 0.10 \text{ g/L}$, $pH = 7.0$, $T = 25 \text{ }^\circ C$.

2.2.2. Influence of Reaction Factors

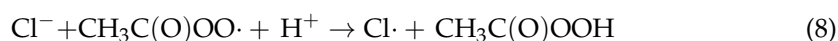
The effect of $CoFe_2O_4$ dosage on OFX degradation is shown in Figure 2b. The removal rates of OFX were 76.2%, 80.4%, 81.9%, and 79.1% when the $CoFe_2O_4$ dose was 0.05, 0.10, 0.20, and 0.40 g/L, respectively. At the same time, the corresponding k_{obs} increased from 0.039 to 0.073 min^{-1} . An increase in surface active sites with increasing $CoFe_2O_4$ accelerates the decomposition of PAA and promotes the generation of ROS. However, $CoFe_2O_4$ itself scavenges ROS when added in excess [35] and causes agglomeration and precipitation, which reduces active sites [21].

The effect of PAA concentration on OFX degradation is shown in Figure 2c. The removal rate of OFX increased from 44.6% to 85.9% when the PAA concentration was raised from 0.1 mM to 0.8 mM, and the k_{obs} also grew by 3.2 times. The increase in PAA concentration can fully utilize the active sites of CoFe_2O_4 to produce more ROS. Nevertheless, the formation of ROS is relatively slowed when active sites are saturated with PAA because of the high PAA concentration. Furthermore, too much PAA has a quenching impact on ROS [21,36].

The pH is a critical factor affecting OFX removal in the $\text{CoFe}_2\text{O}_4/\text{PAA}$ system. The effects of different initial pH on OFX degradation are shown in Figure 2d. In neutral conditions, OFX degraded significantly better than in acidic or alkaline conditions. pH determines the morphology of PAA in aqueous solutions. Since PAA has a pK_a of 8.2, it mostly resides in its neutral form (PAA^0) when the pH is below 8.2, and in its deprotonated form (PAA^-) when the pH is above 8.2 [15]. In addition, pH also affects the surface charge of CoFe_2O_4 whose isoelectric point is 6.5 (Figure S2). Therefore, PAA in solution mainly exists in the form of PAA^- under alkaline conditions, while the surface of CoFe_2O_4 is negatively charged and electrically repulsive, which reduces the chance of contact between PAA and CoFe_2O_4 . Acidic conditions cause the surface of CoFe_2O_4 to become positively charged, and the O-O bond of PAA can easily form a hydrogen bond with H^+ to become positively charged [37].

2.2.3. Influence of Water Matrix

The widespread presence of anions and dissolved organic matter (DOM) in the aqueous environment could affect OFX degradation by scavenging ROS and forming complexes with metal ions. As shown in Figure 2e, Cl^- and SO_4^{2-} have a slight effect on OFX degradation in the $\text{CoFe}_2\text{O}_4/\text{PAA}$ system. As SO_4^{2-} typically does not react with ROS ($\cdot\text{OH}$, $\text{R-O}\cdot$), its presence in high quantities has no significant impact on OFX removal. According to previous studies, Cl^- generally plays two roles in the PAA system: (i) Cl^- can react directly with PAA to produce the secondary oxidant HOCl (Equation (7)) [38], and (ii) Cl^- also reacts with ROS to form chlorine-containing reactive species ($\text{Cl}\cdot$, $\text{HOCl}\cdot^-$, $\text{Cl}_2\cdot^-$) (Equations (8)–(11)), which have different sensitivities to different pollutants [39].



High concentrations of NO_3^- significantly inhibited the degradation of OFX. It is possible that NO_3^- reacts with reactive radicals to generate NO_2^- , which also competes with OFX for ROS [40]. Obviously, HCO_3^- strongly suppressed the degradation of OFX. The removal rates of OFX were only 69.3%, 15.7%, 10.5%, and 9.0% when the concentration of HCO_3^- in the system was 1, 5, 10, and 20 mM, respectively. HCO_3^- is a common scavenger of $\cdot\text{OH}$ and hardly reacts with $\text{R-O}\cdot$, therefore the inhibitory effect on OFX degradation is not a competition for reactive radicals [16]. As previously reported, the CoFe_2O_4 surface forms a Co-HCO_3^- complex with HCO_3^- , which blocks PAA activation [16,41]. Moreover, HCO_3^- is a buffer substance that affects the pH in the reaction system [18], and the weak alkaline conditions are not favorable for OFX degradation by $\text{CoFe}_2\text{O}_4/\text{PAA}$. HA plays a part in inhibiting the removal of OFX in the $\text{CoFe}_2\text{O}_4/\text{PAA}$ system, especially at high concentrations of HA. HA is a common radical scavenger [39] and can readily adsorb onto the surface of CoFe_2O_4 to form unreactive complexes [30,42].

2.3. Reusability and Stability of the CoFe_2O_4

The reusability of CoFe_2O_4 was evaluated with cycling experiments, which were carried out under the same reaction system. As can be seen from Figure 3a, the removal efficiency of OFX could still be kept over 80% after five cycles, which indicates that CoFe_2O_4 has a stable catalytic performance for PAA. Additionally, the highest leaching amount of cobalt ions was only 0.055 mg/L in cycling experiments (Figure 3b), while iron ions were not detected. Moreover, the XRD and FT-IR analyses of CoFe_2O_4 before and after the reaction also further confirmed the structural stability of CoFe_2O_4 with regard to PAA activation. The superior catalytic and structural stability of CoFe_2O_4 is of great benefit for the application of the $\text{CoFe}_2\text{O}_4/\text{PAA}$ system in practice.

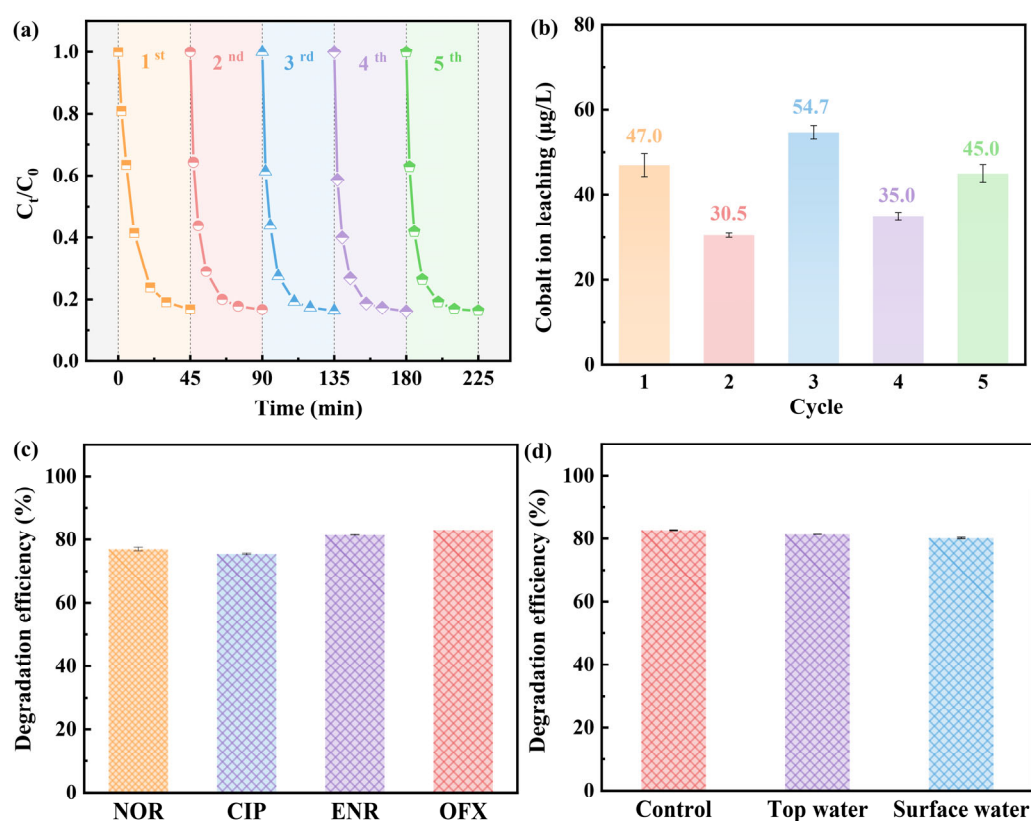


Figure 3. Degradation of OFX (a) and the leaching of cobalt ions during cycling experiments (b); degradation of different FQs (c) and OFX in different water bodies (d) by $\text{CoFe}_2\text{O}_4/\text{PAA}$ system. Experimental conditions: $[\text{OFX}] = [\text{NOR}] = [\text{CIP}] = [\text{ENR}] = 20 \mu\text{M}$, $[\text{PAA}] = 0.4 \text{ mM}$, $\text{CoFe}_2\text{O}_4 = 0.10 \text{ g/L}$, $\text{pH} = 7.0$, $T = 25 \text{ }^\circ\text{C}$.

2.4. Applicability of $\text{CoFe}_2\text{O}_4/\text{PAA}$ System

The degradation effect of the $\text{CoFe}_2\text{O}_4/\text{PAA}$ system on other three different FQs was investigated and the results are shown in Figure 3c. Norfloxacin (NOR), Ciprofloxacin (CIP), and Enrofloxacin (ENR) were degraded to a great extent after 45 min and the removal rates could reach 77.0%, 75.5%, and 81.5%, respectively, suggesting that the $\text{CoFe}_2\text{O}_4/\text{PAA}$ system has the same great degradation performance as other FQs. In addition, the performance of the $\text{CoFe}_2\text{O}_4/\text{PAA}$ process for OFX degradation was evaluated in both tap water and surface water. It was pleasantly surprising that the removal efficiency of OFX in tap water and surface water was decreased by only 1.4% and 2.5%, respectively (Figure 3d). The information about these two water types is listed in Table S2. The reason for this slight inhibition may be that coexisting ions and organic matter in actual water can consume ROS. Thereby, the $\text{CoFe}_2\text{O}_4/\text{PAA}$ process has promising potential for practical application.

2.5. Identification and Analysis of Reactive Species

It has been reported that various reactive species might be involved in PAA-based AOPs, such as $\cdot\text{OH}$, $\text{O}_2^{\cdot-}$, $^1\text{O}_2$, $\text{R}\cdot\text{O}$ ($\text{CH}_3\text{C}(\text{O})\text{O}\cdot$, $\text{CH}_3\text{C}(\text{O})\text{OO}\cdot$) and high-valent metal species (Co (IV), Fe (IV)) [16,43]. Therefore, a quenching experiment was conducted to identify ROS produced in the $\text{CoFe}_2\text{O}_4/\text{PAA}$ system. Tertiary butyl alcohol (TBA) is a typical $\cdot\text{OH}$ scavenger at a high reaction rate with $\cdot\text{OH}$ ($k_{\text{TBA}/\cdot\text{OH}} = 6.0 \times 10^8 \text{ M}^{-1}\text{s}^{-1}$) [44]. As shown in Figure 4a, the addition of excess TBA slightly inhibited the removal of OFX, indicating the minor role of $\cdot\text{OH}$ in the system. MeOH serves as a common scavenger for both $\cdot\text{OH}$ ($k_{\text{MeOH}/\cdot\text{OH}} = 9.7 \times 10^8 \text{ M}^{-1}\text{s}^{-1}$) and $\text{R}\cdot\text{O}$ in the PAA system [32]. Hence, the contributions of $\cdot\text{OH}$ and $\text{R}\cdot\text{O}$ to the degradation of OFX could be distinguished by the use of TBA and MeOH. Obviously, too much MeOH could greatly reduce the removal rate of OFX, which fell from 83.1% to 40.3% (Figure 4a). Thus, the inhibition induced by MeOH was attributed to the scavenging effect of $\text{R}\cdot\text{O}$ rather than $\cdot\text{OH}$. To further verify this, *p*CBA ($k_{p\text{CBA}/\cdot\text{OH}} = 5.0 \times 10^9 \text{ M}^{-1}\text{s}^{-1}$) and NAP ($k_{\text{NAP}/\text{R}\cdot\text{O}} = 9.0 \times 10^9 \text{ M}^{-1}\text{s}^{-1}$) were utilized as specific probes for $\cdot\text{OH}$, $\text{R}\cdot\text{O}$ to explore the contribution to OFX degradation [44,45]. As presented in Figure S3, complete removal of NAP occurred within 10 min, whereas only 10% of *p*CBA was degraded after 45 min. This observation evidenced that a large number of $\text{R}\cdot\text{O}$ and less $\cdot\text{OH}$ exist in the $\text{CoFe}_2\text{O}_4/\text{PAA}$ system.

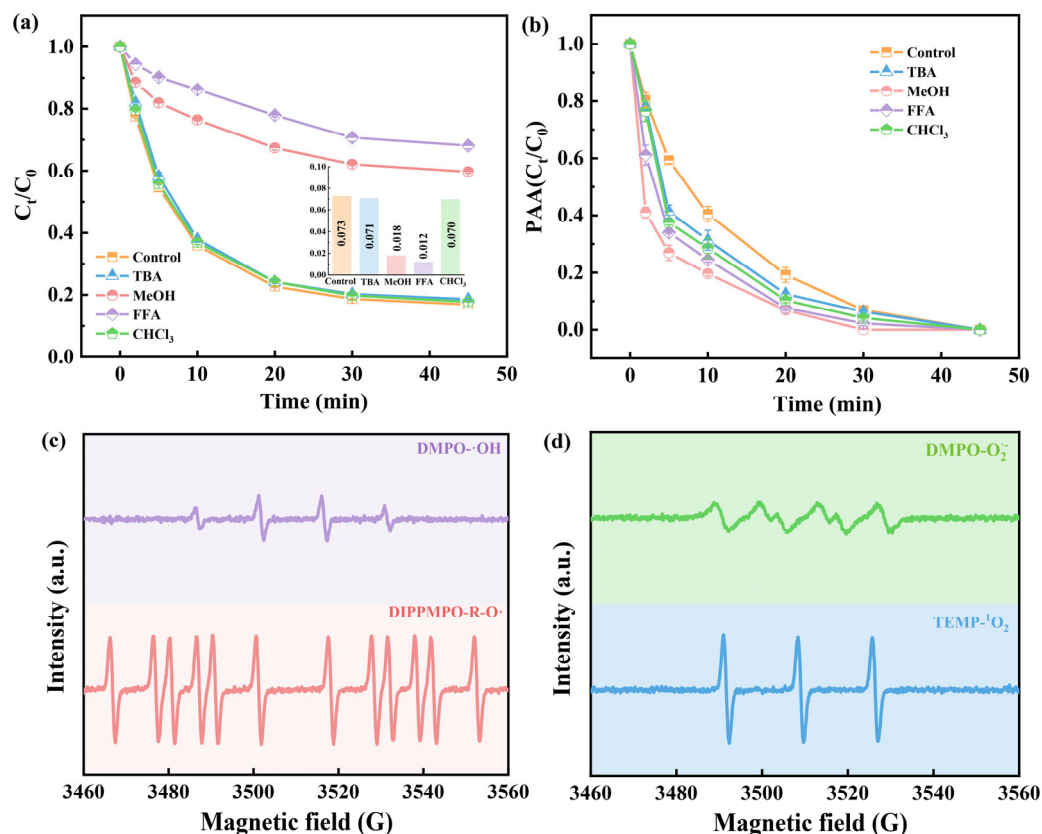


Figure 4. The effect of quenchers on the degradation of OFX (a) and the decomposition of PAA (b) in $\text{CoFe}_2\text{O}_4/\text{PAA}$ system; EPR signal of ROS trapped: $\cdot\text{OH}$ and $\text{R}\cdot\text{O}$ (c) and $\text{O}_2^{\cdot-}$ and $^1\text{O}_2$ (d) in $\text{CoFe}_2\text{O}_4/\text{PAA}$ system. Experimental conditions: $[\text{OFX}] = 20 \mu\text{M}$, $[\text{PAA}] = 0.4 \text{ mM}$, $\text{CoFe}_2\text{O}_4 = 0.10 \text{ g/L}$, $[\text{TBA}] = [\text{MeOH}] = 100 \text{ mM}$, $[\text{FFA}] = [\text{CHCl}_3] = 10 \text{ mM}$, $\text{pH} = 7.0$, $T = 25 \text{ }^\circ\text{C}$.

CHCl_3 can act as a scavenger of $\text{O}_2^{\cdot-}$, which rapidly reacts with $\text{O}_2^{\cdot-}$ ($k_{\text{CHCl}_3/\text{O}_2^{\cdot-}} = 2.3 \times 10^8 \text{ M}^{-1}\text{s}^{-1}$) [44]. The degradation of OFX was not affected by CHCl_3 , which means $\text{O}_2^{\cdot-}$ had little involvement. Additionally, FFA is widely used as a quencher of $^1\text{O}_2$ ($k_{\text{FFA}/^1\text{O}_2} = 1.2 \times 10^8 \text{ M}^{-1}\text{s}^{-1}$) [16]. According to the results in Figure 4a, the inhibitory effect of FFA on OFX degradation is significantly higher than that of other quenchers,

indicating that $^1\text{O}_2$ plays an important role in the degradation process. Meanwhile, the addition of excess quenchers can consume a part of PAA (Figures 4b and S4).

The formation of high-valent metal species like Co(IV) and Fe(IV) in the system could be probed by methyl phenyl sulfoxide (PMSO). PMSO was reported to be converted to methyl phenyl sulfone (PMSO₂) with high-valent metal species via an oxygen atom transfer route [35,46], in contrast to free radicals, which form hydroxylated products [47]. It turned out that PMSO₂ occurred in the CoFe₂O₄/PAA system, but the conversion rate of PMSO to PMSO₂ was only 8.0% (Figure S5). Moreover, the removal rate of OFX was only decreased by 2.5% when excess PMSO was introduced (Figure S6). The results demonstrated that high-valent metal species (Co(IV), Fe(IV)) serve a minor role in OFX degradation.

EPR tests were performed to further verify the generation of ROS in the CoFe₂O₄/PAA system. DMPO is the spin-trapping agent of $\cdot\text{OH}$ and $\text{O}_2^{\cdot-}$, while DIPPMPO and TEMP serve as the trapping agents for R-O \cdot and $^1\text{O}_2$, respectively [45,48]. As shown in Figure 4c,d, the signals of DMPO- $\cdot\text{OH}$ (1:2:2:1), DIPPMPO-R-O \cdot (12 lines), DMPO- $\text{O}_2^{\cdot-}$, and TEMP- $^1\text{O}_2$ (1:1:1) adducts were detected, demonstrating the existence of $\cdot\text{OH}$, R-O \cdot , $\text{O}_2^{\cdot-}$, and $^1\text{O}_2$ in the CoFe₂O₄/PAA system.

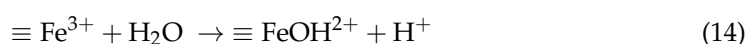
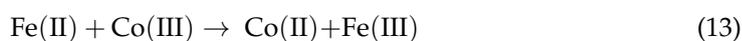
Furthermore, $\text{CH}_3\text{C}(\text{O})\text{O}\cdot$ and $\text{CH}_3\text{C}(\text{O})\text{OO}\cdot$ are two critical R-O \cdot species in PAA-based AOPs that are crucial in pollutant degradation. Generally, $\text{CH}_3\text{C}(\text{O})\text{O}\cdot$ is extremely unstable as a primary radical, susceptible to self-decay to form $\text{CH}_3\cdot$ ($k = 2.3 \times 10^5 \text{ M}^{-1}\text{s}^{-1}$) (Equation (12)) and is less reactive toward most organic compounds [20,49]. In contrast, $\text{CH}_3\text{C}(\text{O})\text{OO}\cdot$ is capable of strong oxidation [19]. Thus, $\text{CH}_3\text{C}(\text{O})\text{OO}\cdot$ is the main R-O \cdot involved in OFX degradation. Based on the above analysis, it can be inferred that R-O \cdot (especially $\text{CH}_3\text{C}(\text{O})\text{OO}\cdot$) and $^1\text{O}_2$ are the major reactive species responsible for OFX removal in the CoFe₂O₄/PAA system.



2.6. Activation Mechanism

To further illustrate the activation mechanism of CoFe₂O₄ on PAA, XPS analysis of CoFe₂O₄ before and after the reaction was performed. The XPS full spectrum scans of CoFe₂O₄ before and after the reaction are shown in Figure 5a, which reveals the presence of Co, Fe, and O. Figure 5b displays the XPS peak-fitting spectra of Co 2p before and after the reaction of CoFe₂O₄. The Co(III) exhibits distinctive peak positions at 778.9 eV (Co 2p_{3/2}) and 794.1 eV (Co 2p_{1/2}), whereas Co(II) is associated with peak locations at 780.6 eV (Co 2p_{3/2}) and 795.4 eV (Co 2p_{1/2}). The proportion of Co(III) declined from 53.42% to 49.56%, whereas the Co(II) increased from 46.58% to 50.44%. These observations indicate the presence of a redox cycle involving $\equiv\text{Co}(\text{II})/\equiv\text{Co}(\text{III})$ on the surface of CoFe₂O₄ throughout the reaction [18,45].

Figure 5c shows the XPS peak-fitting spectra of Fe 2p before and after the CoFe₂O₄ reaction. The peaks of Fe(II) at Fe 2p_{3/2} and Fe 2p_{1/2} correspond to binding energies of 710.0 eV and 723.4 eV, respectively, while those for Fe(III) are 711.8 eV and 725.1 eV. The proportion of Fe(II) declined from 58.68% to 55.88% and the corresponding increase in Fe(III) from 41.32% to 44.12% suggests the presence of a redox cycle with $\equiv\text{Fe}(\text{III})/\equiv\text{Fe}(\text{II})$ on the CoFe₂O₄. Nevertheless, the involvement of $\equiv\text{Fe}(\text{III})/\equiv\text{Fe}(\text{II})$ in the activation of PAA is minimal in comparison to $\equiv\text{Co}(\text{II})/\equiv\text{Co}(\text{III})$ [42]. It should be noticed that the presence of Fe in CoFe₂O₄ promotes the transformation of Co(III) to Co(II) (Equation (13)), which improves the electron-transfer capacity of the catalyst [45].



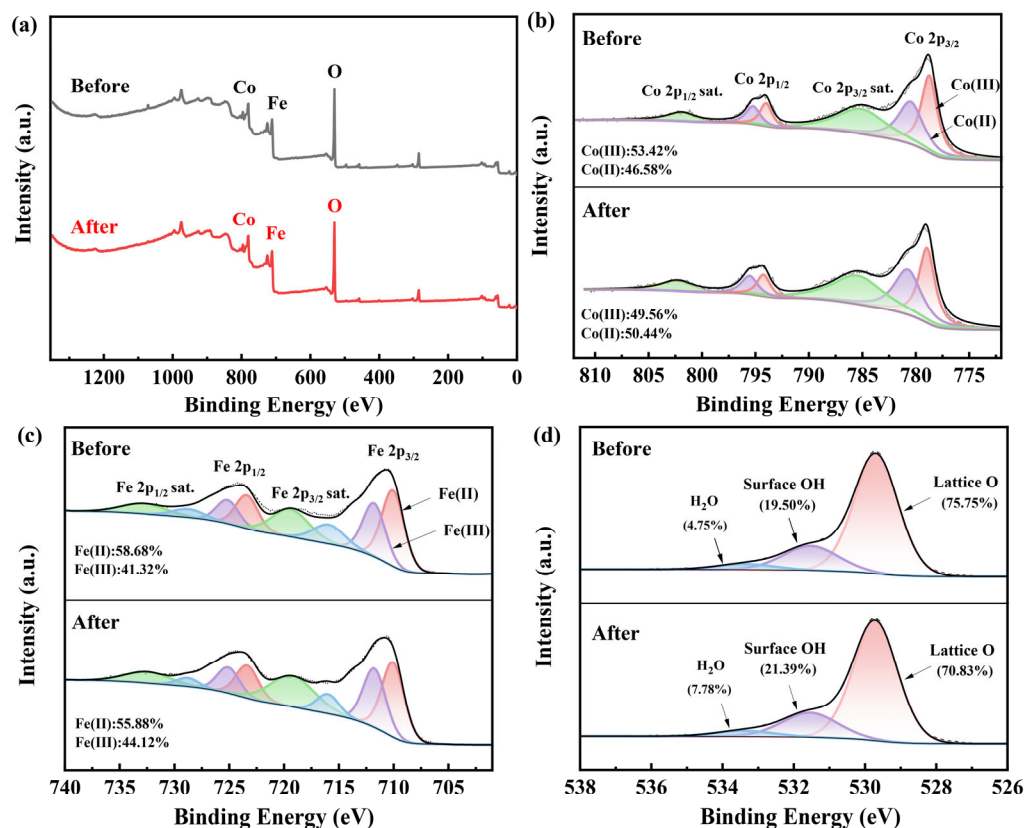
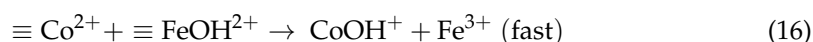
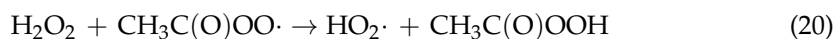
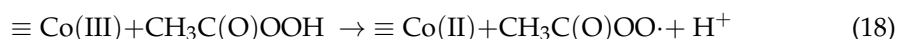


Figure 5. XPS spectra for (a) survey scan, (b) Co 2p, (c) Fe 2p, and (d) O 1s of CoFe₂O₄ before and after the reaction.

As shown in Figure 5d, the peaks of lattice oxygen, surface hydroxyl oxygen, and adsorbed oxygen are located at 529.7 eV, 531.5 eV, and 533.2 eV, respectively. The lattice oxygen decreased from 75.75% to 70.83%, while surface hydroxyl oxygen increased from 19.50% to 21.39%, and adsorbed oxygen rose from 4.75% to 7.78%. The decrease in lattice oxygen can be attributed to the reduction of Co(III) to Co(II), while the increase in surface hydroxyl oxygen can be explained by the formation of Co-OH and Fe-OH (Equations (14)–(16)) [30,42].

Therefore, the degradation of OFX in the CoFe₂O₄/PAA system was attributed to the generation of reactive species, especially R-O[•] and ¹O₂, and Co played an important role in PAA activation. Based on the above discussion, the activation mechanism of CoFe₂O₄ on PAA was proposed. Initially, the surface ≡Co(II) of CoFe₂O₄ donates an electron to PAA, which results in the formation of CH₃C(O)O[•] and the conversion of ≡Co(II) to ≡Co(III). Subsequently, the generated ≡Co(III) would receive an electron from PAA and recover to ≡Co(II), accompanied by the formation of CH₃C(O)OO[•]. Therefore, the ≡Co(II)/≡Co(III) redox cycle is repeated on the catalyst surface to generate R-O[•] for the degradation of OFX (Equations (17) and (18)). Additionally, the coexisting H₂O₂ reacts with R-O[•] (CH₃C(O)O[•], CH₃C(O)OO[•]) to produce HO₂[•] (Equations (19) and (20)), which has a weak oxidizing capacity and is prone to forming O₂^{•-} by deprotonation (Equation (21)). Moreover, ¹O₂ could be obtained from the recombination of O₂^{•-} (Equation (22)). Although the role of Fe in the activation of PAA might be disregarded, the interaction of Fe with Co speeds up the rate of electron transfer at the catalytic interface as well as the adsorption of PAA [42,45].





2.7. Degradation Pathway and Toxicity Assessment

Three-dimensional fluorescence spectroscopy (3D-EEM) was used to observe the compositional changes of organic matter during OFX degradation and to perform a preliminary analysis of the evolution of the molecular structure. As shown in Figure 6a, OFX showed double fluorescence peaks. The two peaks were located in the ranges of $E_x/E_m = (275\text{--}300\text{ nm})/(400\text{--}575\text{ nm})$ and $E_x/E_m = (300\text{--}375\text{ nm})/(400\text{--}575\text{ nm})$, which belong to humic acid-like substances. Meanwhile, it further reflects the aromatic structure of OFX and functional groups such as carboxyl groups (-COOH) and carbonyl groups (-C=O) [50]. As the reaction went on, the intensity of the two fluorescence peaks gradually weakened and the center of the peaks was slightly shifted to the left (Figure 6a–d), implying that the conjugated structure of OFX was continuously destroyed to form intermediate products and that the $\text{CoFe}_2\text{O}_4/\text{PAA}$ system could degrade OFX effectively.

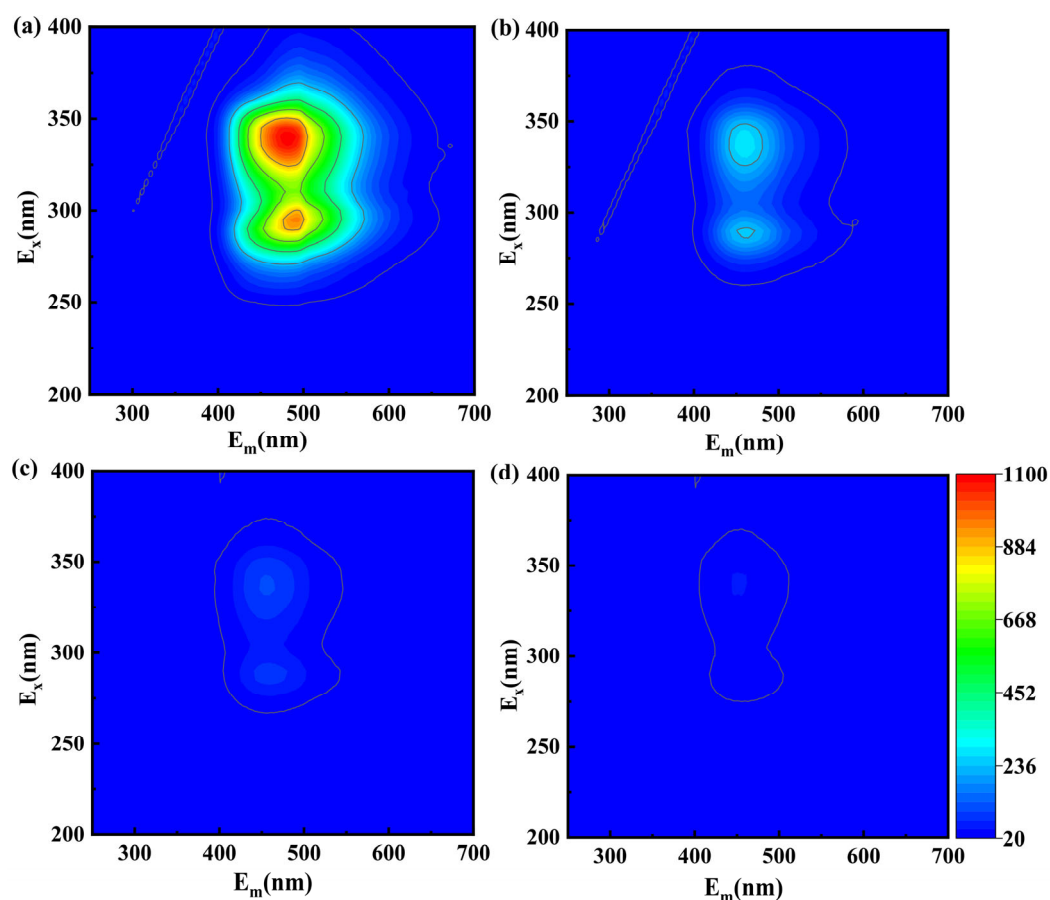


Figure 6. Three-dimensional fluorescence spectra (3D-EEM) at different times during the degradation of OFX by $\text{CoFe}_2\text{O}_4/\text{PAA}$ system: (a) 0 min, (b) 10 min, (c) 20 min, (d) 45 min. Experimental conditions: $[\text{OFX}] = 20\ \mu\text{M}$, $[\text{PAA}] = 0.4\ \text{mM}$, $\text{CoFe}_2\text{O}_4 = 0.10\ \text{g/L}$, $\text{pH} = 7.0$, $T = 25\ ^\circ\text{C}$.

The degradation intermediates of OFX in the $\text{CoFe}_2\text{O}_4/\text{PAA}$ system were detected by LC-TOF-MS (Figure S7) and summarized in Table S4. Four possible degradation pathways of OFX were proposed based on experimental results and related literature (Figure 7). In pathway I, opening of the oxazine ring and hydroxylation of the quinolone moiety in OFX occurred to form P1 ($m/z = 354$), followed by the generation of P2 ($m/z = 314$) via the cleavage of C=C and C-N bonds, and was further demethylated to produce P3 ($m/z = 283$) [51]. In pathway II, decarboxylation and hydroxylation of the quinolone moiety in OFX formed P4 ($m/z = 334$), and P4 was oxidized to produce P5 ($m/z = 205$), which was transformed to P6 ($m/z = 194$) via the cleavage of the C=C bond and hydroxylation [52,53]. In pathway III, P7 ($m/z = 280$) was obtained by the epoxidation and hydroxylation of piperazine from OFX and was then further converted to P8 ($m/z = 224$) via decarboxylation, deamination, and demethylation. As part of pathway IV, OFX was first defluorinated to form P9 ($m/z = 344$), followed by the generation of P10 ($m/z = 327$) and P11 ($m/z = 300$) via demethylation and decarboxylation, respectively, and P12 ($m/z = 149$) was obtained by the ring-opening of P11 [51,52]. Eventually, these intermediates are mineralized into inorganic molecules such as CO_2 , H_2O , NO_3^- , and F^- . As a whole, ring opening, decarboxylation, defluorination, hydroxylation, demethylation, and bond cleavage contribute to OFX degradation.

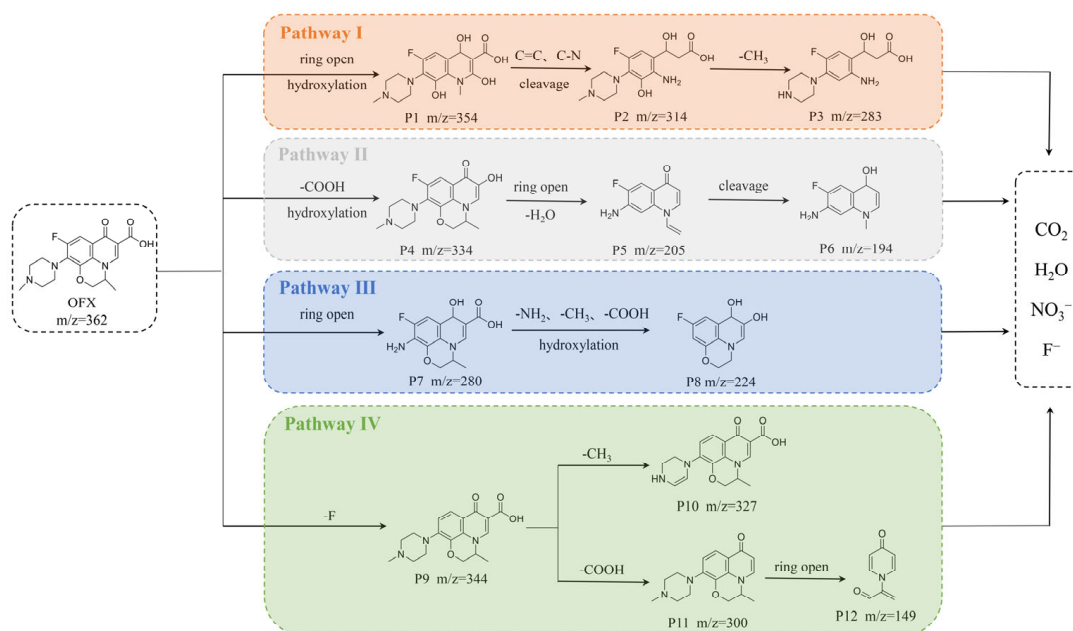


Figure 7. The possible degradation pathway of OFX in $\text{CoFe}_2\text{O}_4/\text{PAA}$ system.

To evaluate the toxicity variation, toxicity software (T.E.S.T., Version 5.1.2) based on quantitative structure–activity relationship (QSAR) was applied to predict the ecotoxicity of OFX and its detected intermediates, which include acute toxicity, bioconcentration factors, developmental toxicity, and mutagenicity. It is worth mentioning that OFX exhibited toxicity, as seen by its 96 h Fathead minnow LC_{50} value of 1.24 mg/L (Figure 8a). This value was lower than that of the intermediates, suggesting a significant reduction in acute toxicity following degradation. As displayed in Figure 8b, the obtained bioaccumulation factor of OFX and its intermediates indicated that all intermediates except P1, P2, P3, P7, and P10 were lower than OFX. Additionally, the developmental toxicity value of OFX was higher than most of the intermediates (Figure 8c), proving a decrease in developmental toxicity after degradation except for P4 and P9, and P12 even showed developmental non-toxicants. OFX and most of the intermediates were classified as mutagenicity-positive, and P11 was even considered mutagenicity-negative (Figure 8d). After the reaction, it was found that the total toxicity of OFX was lower than before the reaction, indicating that the $\text{CoFe}_2\text{O}_4/\text{PAA}$ system offered a high-level potential for toxicity reduction.

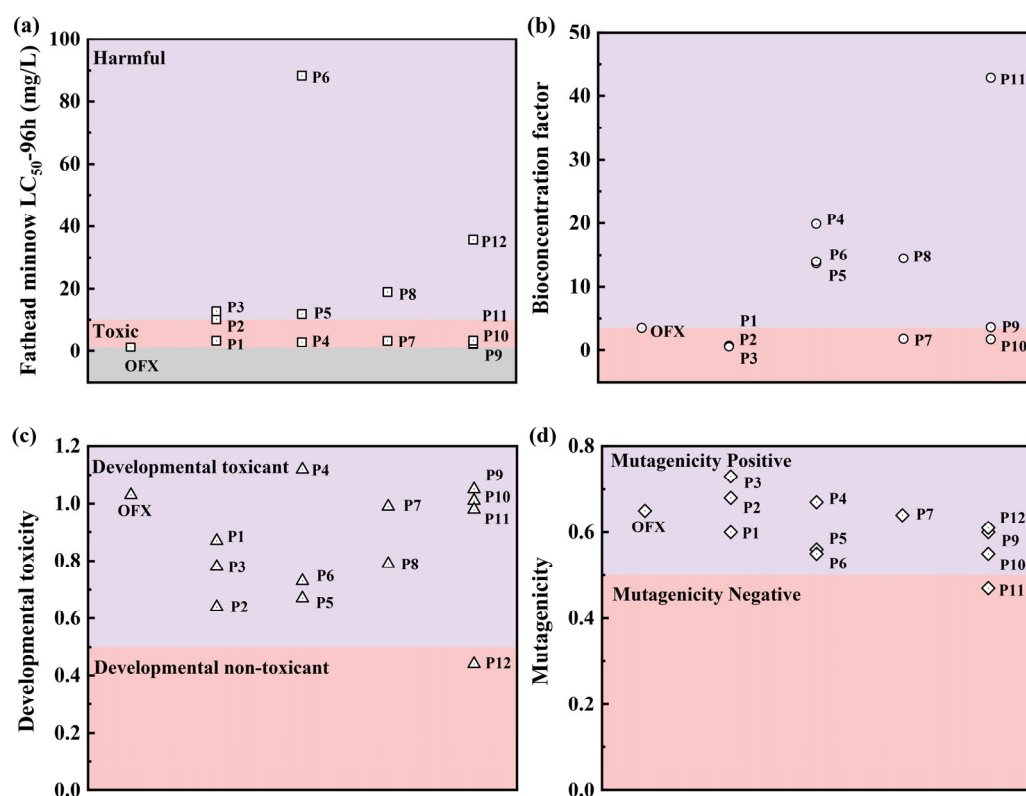


Figure 8. Toxicity assessment of OFX and intermediates: (a) Fathead minnow LC₅₀ (96 h), (b) bioconcentration factor, (c) developmental toxicity, and (d) Ames mutagenicity.

3. Materials and Methods

3.1. Chemicals

Ofloxacin (OFX), Norfloxacin (NOR), Ciprofloxacin (CIP), Enrofloxacin (ENR), Tert-butanol (TBA), Methanol (MeOH), and Trichloromethane (CHCl₃) were purchased from Macklin Biochemical (Shanghai, China). Furfuryl alcohol (FFA), N, N-diethyl-p-phenylenediamine (DPD), Humic acid (HA), *p*-chlorobenzoic acid (*p*CBA), Naproxen (NAP), Methyl phenyl sulfoxide (PMSO), and Methyl phenyl sulfone (PMSO₂) were provided by Aladdin Co., Ltd. (Shanghai, China). Acetonitrile (CH₃CN) and Formic acid (HCOOH) of HPLC grade were purchased from Sinopharm Chemical Reagent Co., Ltd. (Shanghai, China). CoFe₂O₄, whose size was around 100 nm, was supplied by Aladdin Co., Ltd. (Shanghai, China). Commercial PAA stock solution was supplied by Kemiou Chemical Reagent (Tianjin, China), and the molar ratio of PAA to H₂O₂ in the stock solution was 0.7. All other chemicals and reagents were provided by Sinopharm Chemical Reagent Co., Ltd. The CAS registry number of all chemicals is listed in Table S5. All chemicals were of analytical grade and used without further purification.

3.2. Degradation Experiments

Degradation experiments were conducted in a 250 mL glass reactor with shock stirring (Thermostatic shaker SYC-2A, Shanghai Bunting Instrument Co., Shanghai, China) at a speed of 150 rpm. Firstly, 100 mL of 20 μM OFX solution was transferred to the reactor, followed by the addition of a predetermined concentration of PAA, and then the solution's pH was adjusted with diluted H₂SO₄ and NaOH. The experiments were initiated with the addition of CoFe₂O₄. All the experiments were maintained at 23 ± 2 °C. Samples were collected within a predetermined time (0, 2, 5, 10, 20, 30, 45 min), and quenched by Na₂S₂O₃, then filtered with a 0.22 μm aqueous filter membrane for analysis.

Different concentrations of anions (Cl⁻, SO₄²⁻, NO₃⁻, HCO₃⁻) and HA were added to the reaction solution to investigate the effect of water matrices on OFX degradation.

ROS in the system were identified by radical scavengers (TBA, MeOH, CHCl_3 , FFA) and verified by probe compounds (*p*CBA, NAP, PMSO). NOR, CIP, and ENR were used to evaluate the applicability of CoFe_2O_4 /PAA systems for FQs. In order to evaluate the stability of the catalytic performance of CoFe_2O_4 , the used catalyst was desorbed by alkali and then washed with deionized water to neutral and dried at 60 °C. All experiments were conducted at least twice, and the error bar shown in the figure represents the standard deviation between replicates.

The stock solution of OFX (30 mg/L) was obtained by dissolving OFX in pure water with stirring and was stored at 4 °C. The working solution of OFX was diluted from the stock solution. Kinetic analysis of OFX degradation was depicted in Text S1.

3.3. Analytical Methods

The surface morphology and chemical composition of CoFe_2O_4 were characterized using scanning electron microscopy (SEM, Scios 2 HiVac, FEI, Danville, CA, USA) equipped with energy-dispersive X-ray spectroscopy (EDS). The crystal phase structure of CoFe_2O_4 before and after the reaction was determined through an X-ray diffractometer (XRD, Smart-Lab SE, Rigaku, Japan) with Cu-K α radiation over the range of 10° to 80°, and Fourier transform infrared spectroscopy (FT-IR, Nicolet iS20, Thermo Scientific, Waltham, MA, USA) was used to determine functional groups. The surface elemental composition of CoFe_2O_4 before and after the reaction were analyzed by X-ray photoelectron spectroscopy (XPS, K-Alpha, Thermo Scientific, USA), and the zeta potential of CoFe_2O_4 was measured using a Zeta potentiometer (Nano ZS90, Malvern, UK).

The PAA stock solution was calibrated weekly by titration, and the concentrations of peroxide and hydrogen peroxide in the PAA stock solution were determined using iodimetry and potassium permanganate titration, respectively, so as to calculate the concentration of PAA [39]. The residual PAA concentration was determined by N, N-diethyl-p-phenylenediamine (DPD) spectrophotometry [15]. The concentration of OFX, NOR, CIP, ENR, *p*CBA, NAP, PMSO, and PMSO₂ were detected by high-performance liquid chromatography (HPLC, Agilent 1260, Santa Clara, CA, USA) coupled with an Agilent EC-C18 column and the details of the conditions are presented in Table S6. The concentrations of cobalt and iron ions were analyzed using inductively coupled plasma-atomic emission spectrometry (ICP-AES, ICP-5000, Focused Photonics Inc, Shanghai, China), and pH values were measured by a pH meter (pH-FE28, METTLER TOLEDO, Greifensee, Switzerland). Electron paramagnetic resonance (EPR) tests were carried out to verify the generated ROS using 5,5-dimethyl-1-pyrroline N-oxide (DMPO), 5-Diisopropoxyphosphoryl-5-methyl-1-pyrroline N-oxide (DIPPMPO), and 2,2,6,6-tetramethyl-4-piperidiny1 (TEMP) as trapping agents. The detection of three-dimensional fluorescence spectra (3D-EEM) was performed on a fluorescence spectrophotometer (Lengguang F98, Shanghai, China). The intermediates of OFX degradation were determined by LC-QTOF-MS (Agilent 1290-6550, USA) coupled with electrospray ionization (ESI). Meanwhile, the biological toxicity of OFX and its oxidation intermediates was evaluated by the Toxicity Estimation Software Tool (T.E.S.T., Version 5.1.2), which is based on the quantitative structure-activity relationship (QSAR) method.

4. Conclusions

In this study, CoFe_2O_4 displayed remarkable catalytic performance in the activation of PAA for OFX degradation, and a removal efficiency of 83.0% OFX was achieved within 45 min under neutral conditions. The CoFe_2O_4 /PAA system exhibited better resistance to anions and HA at low concentrations in water, but NO_3^- , HCO_3^- , and HA could inhibit OFX degradation at high concentrations. Additionally, CoFe_2O_4 showed excellent catalytic performance in cycling experiments and great potential for practical wastewater treatment. R-O· ($\text{CH}_3\text{C}(\text{O})\text{OO}\cdot$) and $^1\text{O}_2$ played a dominant role in the degradation of OFX, and the $\equiv\text{Co}(\text{II})/\equiv\text{Co}(\text{III})$ redox cycle occurring on the surface of CoFe_2O_4 during the reaction promoted the decomposition of PAA to generate ROS. Finally, the possible degradation pathways of OFX involved ring opening, bond cleavage, decarboxylation, defluorination,

hydroxylation, and demethylation. Toxicity assessment indicated that the CoFe₂O₄/PAA system could effectively reduce the biological toxicity of OFX. This study contributes to the practical application of non-homogeneous PAA-based AOPs in wastewater treatment.

Supplementary Materials: The following supporting information can be downloaded at: <https://www.mdpi.com/article/10.3390/molecules28237906/s1>. Refs. [54–59] are cited in Supplementary Materials.

Author Contributions: Conceptualization, R.L. and S.P.; methodology, R.L., X.L. and S.P.; software, R.L. and X.L.; validation, J.G. and Y.C.; investigation, R.L. and J.G.; writing—original draft preparation, R.L.; writing—review and editing, R.L. and S.P.; visualization, X.L. and J.G.; supervision, Y.C.; funding acquisition, S.P. All authors have read and agreed to the published version of the manuscript.

Funding: This research was funded by the National Natural Science Foundation of China (Grant No. 52000102).

Institutional Review Board Statement: Not applicable.

Informed Consent Statement: Not applicable.

Data Availability Statement: Data are contained within the article and Supplementary Materials.

Acknowledgments: The authors would like to express gratitude to the National Natural Science Foundation of China (Grant No. 52000102) for offering financial support for this research.

Conflicts of Interest: The authors declare that they have no known competing financial interests or personal relationships that could have appeared to influence the work reported in this paper.

References

1. Dan, A.; Zhang, X.M.; Dai, Y.V.; Chen, C.X.; Yang, Y. Occurrence and removal of quinolone, tetracycline, and macrolide antibiotics from urban wastewater in constructed wetlands. *J. Clean. Prod.* **2020**, *252*, 119677.
2. Oberoi, A.S.; Jia, Y.; Zhang, H.; Khanal, S.K.; Lu, H. Insights into the fate and removal of antibiotics in engineered biological treatment systems: A critical review. *Environ. Sci. Technol.* **2019**, *53*, 7234–7264. [[CrossRef](#)] [[PubMed](#)]
3. Zainab, S.M.; Junaid, M.; Xu, N.; Malik, R.N. Antibiotics and antibiotic resistant genes (ARGs) in groundwater: A global review on dissemination, sources, interactions, environmental and human health risks. *Water Res.* **2020**, *187*, 116455. [[CrossRef](#)] [[PubMed](#)]
4. Hoang Quoc, A.; Thi Phuong Quynh, L.; Nhu Da, L.; Lu, X.X.; Thi Thuy, D.; Garnier, J.; Rochelle-Newall, E.; Zhang, S.; Neung-Hwan, O.; Oeurng, C.; et al. Antibiotics in surface water of East and Southeast Asian countries: A focused review on contamination status, pollution sources, potential risks, and future perspectives. *Sci. Total Environ.* **2021**, *764*, 142856.
5. Yang, C.D.; Wu, T.Y. A comprehensive review on quinolone contamination in environments: Current research progress. *Environ. Sci. Pollut. Res.* **2023**, *30*, 48778–48792. [[CrossRef](#)]
6. Jiao, S.J.; Zheng, S.R.; Yin, D.Q.; Wang, L.H.; Chen, L.Y. Aqueous photolysis of tetracycline and toxicity of photolytic products to luminescent bacteria. *Chemosphere* **2008**, *73*, 377–382. [[CrossRef](#)] [[PubMed](#)]
7. Boxall, A.B.A.; Fogg, L.A.; Blackwell, P.A.; Blackwell, P.; Kay, P.; Pemberton, E.J.; Croxford, A. Veterinary Medicines in the Environment. In *Reviews of Environmental Contamination and Toxicology*; Springer: New York, NY, USA, 2004; pp. 1–91.
8. Yuan, Q.B.; Qu, S.Y.; Li, R.; Huo, Z.Y.; Gao, Y.; Luo, Y. Degradation of antibiotics by electrochemical advanced oxidation processes (EAOPs): Performance, mechanisms, and perspectives. *Sci. Total Environ.* **2023**, *856*, 159092. [[CrossRef](#)]
9. Anjali, R.; Shanthakumar, S. Insights on the current status of occurrence and removal of antibiotics in wastewater by advanced oxidation processes. *J. Environ. Manag.* **2019**, *246*, 51–62. [[CrossRef](#)] [[PubMed](#)]
10. Li, S.; Wu, Y.A.; Zheng, H.S.; Li, H.B.; Zheng, Y.J.; Nan, J.; Ma, J.; Nagarajan, D.; Chang, J.S. Antibiotics degradation by advanced oxidation process (AOPs): Recent advances in ecotoxicity and antibiotic-resistance genes induction of degradation products. *Chemosphere* **2023**, *311*, 136977. [[CrossRef](#)]
11. Wang, J.L.; Zhuan, R. Degradation of antibiotics by advanced oxidation processes: An overview. *Sci. Total Environ.* **2020**, *701*, 135023. [[CrossRef](#)]
12. Luukkonen, T.; Pehkonen, S.O. Peracids in water treatment: A critical review. *Crit. Rev. Environ. Sci. Technol.* **2017**, *47*, 1–39. [[CrossRef](#)]
13. Du, P.H.; Liu, W.; Cao, H.B.; Zhao, H.; Huang, C.H. Oxidation of amino acids by peracetic acid: Reaction kinetics, pathways and theoretical calculations. *Water Res.* **2018**, *1*, 100002. [[CrossRef](#)]
14. Henao, L.D.; Turolla, A.; Antonelli, M. Disinfection by-products formation and ecotoxicological effects of effluents treated with peracetic acid: A review. *Chemosphere* **2018**, *213*, 25–40. [[CrossRef](#)]
15. Cai, M.; Sun, P.; Zhang, L.; Huang, C.-H. UV/Peracetic acid for degradation of pharmaceuticals and reactive species evaluation. *Environ. Sci. Technol.* **2017**, *51*, 14217–14224, Erratum in *Environ. Sci. Technol.* **2020**, *54*, 627. [[CrossRef](#)] [[PubMed](#)]

16. Wang, Z.; Wang, J.; Xiong, B.; Bai, F.; Wang, S.; Wan, Y.; Zhang, L.; Xie, P.; Wiesner, M.R. Application of cobalt/peracetic acid to degrade sulfamethoxazole at neutral condition: Efficiency and mechanisms. *Environ. Sci. Technol.* **2020**, *54*, 464–475. [[CrossRef](#)] [[PubMed](#)]
17. Ao, X.-w.; Eloranta, J.; Huang, C.-H.; Santoro, D.; Sun, W.-j.; Lu, Z.-d.; Li, C. Peracetic acid-based advanced oxidation processes for decontamination and disinfection of water: A review. *Water Res.* **2021**, *188*, 116479. [[CrossRef](#)]
18. Shen, P.; Hou, K.; Chen, F.; Pi, Z.; He, L.; Chen, S.; Li, X.; Yang, Q. Ultra-rapid and long-lasting activation of peracetic acid by Cu-Co spinel oxides for eliminating organic contamination: Role of radical and non-radical catalytic oxidation. *Chem. Eng. J.* **2023**, *463*, 142344. [[CrossRef](#)]
19. Kim, J.; Du, P.; Liu, W.; Luo, C.; Zhao, H.; Huang, C.-H. Cobalt/Peracetic acid: Advanced oxidation of aromatic organic compounds by acetylperoxyl radicals. *Environ. Sci. Technol.* **2020**, *54*, 5268–5278. [[CrossRef](#)]
20. Zhang, L.L.; Chen, J.B.; Zheng, T.L.; Xu, Y.; Liu, T.C.; Yin, W.J.; Zhang, Y.L.; Zhou, X.F. Co-Mn spinel oxides trigger peracetic acid activation for ultrafast degradation of sulfonamide antibiotics: Unveiling critical role of Mn species in boosting Co activity. *Water Res.* **2023**, *229*, 119462. [[CrossRef](#)]
21. Wang, S.; Wang, H.; Liu, Y.; Fu, Y. Effective degradation of sulfamethoxazole with Fe²⁺-zeolite/peracetic acid. *Sep. Purif. Technol.* **2020**, *233*, 115973. [[CrossRef](#)]
22. Rokhina, E.V.; Makarova, K.; Lahtinen, M.; Golovina, E.A.; Van As, H.; Virkutyte, J. Ultrasound-assisted MnO₂ catalyzed homolysis of peracetic acid for phenol degradation: The assessment of process chemistry and kinetics. *Chem. Eng. J.* **2013**, *221*, 476–486. [[CrossRef](#)]
23. Hu, P.D.; Long, M.C. Cobalt-catalyzed sulfate radical-based advanced oxidation: A review on heterogeneous catalysts and applications. *Appl. Catal. B Environ.* **2016**, *181*, 103–117. [[CrossRef](#)]
24. Wang, J.; Wang, Z.; Cheng, Y.; Cao, L.; Bai, F.; Yue, S.; Xie, P.; Ma, J. Molybdenum disulfide (MoS₂): A novel activator of peracetic acid for the degradation of sulfonamide antibiotics. *Water Res.* **2021**, *201*, 117291. [[CrossRef](#)]
25. Liu, P.; Yao, Z.; Zhou, J.; Yang, Z.; Kong, L.B. Small magnetic Co-doped NiZn ferrite/graphene nanocomposites and their dual-region microwave absorption performance. *J. Mater. Chem. C.* **2016**, *4*, 9738–9749. [[CrossRef](#)]
26. Yang, H.; Yang, X.; Lin, J.; Yang, F.; He, Y.; Lin, Q. Effect of Cd²⁺ substitution on structural–magnetic and dielectric properties of Ni–Cu–Zn spinel ferrite nanomaterials by Sol–Gel. *Molecules* **2023**, *28*, 6110. [[CrossRef](#)] [[PubMed](#)]
27. Yalçiner, F.; Çevik, E.; Şenel, M.; Baykal, A. Development of an amperometric hydrogen peroxide biosensor based on the immobilization of horseradish peroxidase onto nickel ferrite nanoparticle-chitosan composite. *Nanomicro Lett.* **2011**, *3*, 91–98. [[CrossRef](#)]
28. Su, S.N.; Guo, W.L.; Leng, Y.Q.; Yi, C.L.; Ma, Z.M. Heterogeneous activation of Oxone by Co_xFe_{3-x}O₄ nanocatalysts for degradation of rhodamine B. *J. Hazard. Mater.* **2013**, *244*, 736–742. [[CrossRef](#)]
29. Ren, Y.; Lin, L.; Ma, J.; Yang, J.; Feng, J.; Fan, Z. Sulfate radicals induced from peroxymonosulfate by magnetic ferrosin MF₂O₄ (M=Co, Cu, Mn, and Zn) as heterogeneous catalysts in the water. *Appl. Catal. B Environ.* **2015**, *165*, 572–578. [[CrossRef](#)]
30. Wang, J.W.; Xiong, B.; Miao, L.; Wang, S.L.; Xie, P.C.; Wang, Z.P.; Ma, J. Applying a novel advanced oxidation process of activated peracetic acid by CoFe₂O₄ to efficiently degrade sulfamethoxazole. *Appl. Catal. B Environ.* **2021**, *280*, 119422. [[CrossRef](#)]
31. Zhou, G.; Fu, Y.; Zhou, R.; Zhang, L.; Zhang, L.; Deng, J.; Liu, Y. Efficient degradation of organic contaminants by magnetic cobalt ferrite combined with peracetic acid. *Process Saf. Environ. Prot.* **2022**, *160*, 376–384. [[CrossRef](#)]
32. Dong, J.; Xu, W.; Liu, S.; Gong, Y.; Yang, T.; Du, L.; Chen, Q.; Tan, X.; Liu, Y. Lignin-derived biochar to support CoFe₂O₄: Effective activation of peracetic acid for sulfamethoxazole degradation. *Chem. Eng. J.* **2022**, *430*, 132868. [[CrossRef](#)]
33. Niu, P.; Li, C.H.; Wang, D.Q.; Jia, C.X.; Zhao, J.; Liu, Z.M.; Zhang, X.L.; Geng, L.L. Electronic modulation of fiber-shaped-CoFe₂O₄ via Mg doping for improved PMS activation and sustainable degradation of organic pollutants. *Appl. Surf. Sci.* **2022**, *605*, 154732. [[CrossRef](#)]
34. Zheng, C.; Wu, J.Y.; Zhang, Y.J.; Yang, Q.; Yang, Y.C. Walnut shell loaded with cobalt ferrite as efficient peroxymonosulfate activator to degrade ofloxacin. *Water Air Soil Pollut.* **2023**, *234*, 305. [[CrossRef](#)]
35. Kim, J.; Zhang, T.Q.; Liu, W.; Du, P.H.; Dobson, J.T.; Huang, C.H. Advanced oxidation process with peracetic acid and Fe(II) for contaminant degradation. *Environ. Sci. Technol.* **2019**, *53*, 13312–13322. [[CrossRef](#)]
36. Zhao, Z.; Li, X.; Li, H.; Qian, J.; Pan, B. New insights into the activation of peracetic acid by Co(II): Role of Co(II)-peracetic acid complex as the dominant intermediate oxidant. *ACS ES&T Engg.* **2021**, *1*, 1432–1440.
37. Wu, W.; Tian, D.; Liu, T.C.; Chen, J.B.; Huang, T.Y.; Zhou, X.F.; Zhang, Y.L. Degradation of organic compounds by peracetic acid activated with Co₃O₄: A novel advanced oxidation process and organic radical contribution. *Chem. Eng. J.* **2020**, *394*, 124938. [[CrossRef](#)]
38. Shah, A.D.; Liu, Z.Q.; Salhi, E.; Hofer, T.; von Gunten, U. Peracetic acid oxidation of saline waters in the absence and presence of H₂O₂: Secondary oxidant and disinfection byproduct formation. *Environ. Sci. Technol.* **2015**, *49*, 1698–1705. [[CrossRef](#)] [[PubMed](#)]
39. Chen, S.; Cai, M.; Liu, Y.; Zhang, L.; Feng, L. Effects of water matrices on the degradation of naproxen by reactive radicals in the UV/peracetic acid process. *Water Res.* **2019**, *150*, 153–161. [[CrossRef](#)]
40. Ghanbari, F.; Giannakis, S.; Lin, K.-Y.A.; Wu, J.; Madihi-Bidgoli, S. Acetaminophen degradation by a synergistic peracetic acid/UVC-LED/Fe(II) advanced oxidation process: Kinetic assessment, process feasibility and mechanistic considerations. *Chemosphere* **2021**, *263*, 128119. [[CrossRef](#)]

41. Xu, A.; Li, X.; Ye, S.; Yin, G.; Zeng, Q. Catalyzed oxidative degradation of methylene blue by in situ generated cobalt (II)-bicarbonate complexes with hydrogen peroxide. *Appl. Catal. B Environ.* **2011**, *102*, 37–43. [[CrossRef](#)]
42. Meng, L.; Dong, J.; Chen, J.; Li, L.; Huang, Q.; Lu, J. Activation of peracetic acid by spinel FeCo_2O_4 nanoparticles for the degradation of sulfamethoxazole. *Chem. Eng. J.* **2023**, *456*, 141084. [[CrossRef](#)]
43. Li, S.; Yang, Y.; Zheng, H.; Zheng, Y.; He, C.-S.; Lai, B.; Ma, J.; Nan, J. Introduction of oxygen vacancy to manganese ferrite by Co substitution for enhanced peracetic acid activation and $^1\text{O}_2$ dominated tetracycline hydrochloride degradation under microwave irradiation. *Water Res.* **2022**, *225*, 119176. [[CrossRef](#)] [[PubMed](#)]
44. Guo, Y.; Long, J.; Huang, J.; Yu, G.; Wang, Y. Can the commonly used quenching method really evaluate the role of reactive oxygen species in pollutant abatement during catalytic ozonation? *Water Res.* **2022**, *215*, 118275. [[CrossRef](#)] [[PubMed](#)]
45. Xie, Z.H.; He, C.S.; He, Y.L.; Yang, S.R.; Yu, S.Y.; Xiong, Z.K.; Du, Y.; Liu, Y.; Pan, Z.C.; Yao, G.; et al. Peracetic acid activation via the synergic effect of Co and Fe in CoFe-LDH for efficient degradation of pharmaceuticals in hospital wastewater. *Water Res.* **2023**, *232*, 119666. [[CrossRef](#)] [[PubMed](#)]
46. Liu, B.; Guo, W.; Jia, W.; Wang, H.; Si, Q.; Zhao, Q.; Luo, H.; Jiang, J.; Ren, N. Novel nonradical oxidation of sulfonamide antibiotics with Co(II)-doped g- C_3N_4 -activated peracetic acid: Role of high-valent cobalt-oxo species. *Environ. Sci. Technol.* **2021**, *55*, 12640–12651. [[CrossRef](#)] [[PubMed](#)]
47. Liu, B.; Guo, W.; Jia, W.; Wang, H.; Zheng, S.; Si, Q.; Zhao, Q.; Luo, H.; Jiang, J.; Ren, N. Insights into the oxidation of organic contaminants by Co(II) activated peracetic acid: The overlooked role of high-valent cobalt-oxo species. *Water Res.* **2021**, *201*, 117313. [[CrossRef](#)]
48. Chen, L.; Duan, J.; Du, P.; Sun, W.; Lai, B.; Liu, W. Accurate identification of radicals by in-situ electron paramagnetic resonance in ultraviolet-based homogenous advanced oxidation processes. *Water Res.* **2022**, *221*, 118747. [[CrossRef](#)]
49. Du, P.; Wang, J.; Sun, G.; Chen, L.; Liu, W. Hydrogen atom abstraction mechanism for organic compound oxidation by acetylperoxyl radical in Co(II)/peracetic acid activation system. *Water Res.* **2022**, *212*, 118113. [[CrossRef](#)]
50. Chen, W.; Westerhoff, P.; Leenheer, J.A.; Booksh, K. Fluorescence excitation—emission matrix regional integration to quantify spectra for dissolved organic matter. *Environ. Sci. Technol.* **2003**, *37*, 5701–5710. [[CrossRef](#)]
51. Chen, P.; Gou, Y.J.; Ni, J.M.; Liang, Y.M.; Yang, B.Q.; Jia, F.F.; Song, S.X. Efficient ofloxacin degradation with Co(II)-doped MoS_2 nano-flowers as PMS activator under visible-light irradiation. *Chem. Eng. J.* **2020**, *401*, 125978. [[CrossRef](#)]
52. Li, Y.C.; Wu, Y.H.; Jiang, H.S.; Wang, H. In situ stable growth of Bi_2WO_6 on natural hematite for efficient antibiotic wastewater purification by photocatalytic activation of peroxydisulfate. *Chem. Eng. J.* **2022**, *446*, 136704. [[CrossRef](#)]
53. Xie, Y.X.; Yu, Y.; Xie, H.D.; Huang, F.; Hughes, T.C. 3D-printed heterogeneous Cu_2O monoliths: Reusable supports for antibiotic treatment of wastewater. *J. Hazard. Mater.* **2022**, *436*, 129170. [[CrossRef](#)] [[PubMed](#)]
54. Ye, H.; Xia, L.; Wang, Y.; Zhou, H.; Xie, X.; Zuo, G.; Wu, K. Magnetic $\text{Ag}_3\text{PO}_4/\text{CoFe}_2\text{O}_4$ Z-scheme heterojunction material for photocatalytic decomposition of ofloxacin. *J. Mater. Sci. Mater. Electron.* **2023**, *34*, 2090. [[CrossRef](#)]
55. Singh, S.; Kaur, P.; Kumar, V.; Tikoo, K.B.; Singhal, S. Traversing the advantageous role of samarium doped spinel nanoferrites for photocatalytic removal of organic pollutants. *J. Rare Earths.* **2021**, *39*, 781–789. [[CrossRef](#)]
56. Cao, X.Q.; Xiao, F.; Lyu, Z.W.; Xie, X.Y.; Zhang, Z.X.; Dong, X.; Wang, J.X.; Lyu, X.J.; Zhang, Y.Z.; Liang, Y. CuFe_2O_4 supported on montmorillonite to activate peroxydisulfate for efficient ofloxacin degradation. *J. Water Process. Eng.* **2021**, *44*, 102359. [[CrossRef](#)]
57. Dhiman, P.; Sharma, G.; Alodhayb, A.N.; Kumar, A.; Rana, G.; Sithole, T.; Alothman, Z.A. Constructing a visible-active $\text{CoFe}_2\text{O}_4@/\text{Bi}_2\text{O}_3/\text{NiO}$ nanoheterojunction as magnetically recoverable photocatalyst with boosted ofloxacin degradation efficiency. *Molecules* **2022**, *27*, 8234. [[CrossRef](#)]
58. Nitansh; Kaur, P.; Garg, T.; Renu; Deepika; Kumar, V.; Tikoo, K.; Kaushik, A.; Singhal, S. A fluorescent biomass derived cellulose/PANI/ NiFe_2O_4 composite for the mitigation of toxic pollutants and Cr(VI) sensing from aqueous environment. *J. Ind. Eng. Chem.* **2023**, *129*, 456–473. [[CrossRef](#)]
59. Qin, H.; Cheng, H.; Li, H.; Wang, Y. Degradation of ofloxacin, amoxicillin and tetracycline antibiotics using magnetic core-shell $\text{MnFe}_2\text{O}_4@\text{C-NH}_2$ as a heterogeneous fenton catalyst. *Chem. Eng. J.* **2020**, *396*, 125304. [[CrossRef](#)]

Disclaimer/Publisher's Note: The statements, opinions and data contained in all publications are solely those of the individual author(s) and contributor(s) and not of MDPI and/or the editor(s). MDPI and/or the editor(s) disclaim responsibility for any injury to people or property resulting from any ideas, methods, instructions or products referred to in the content.